Research Square

Preprints are preliminary reports that have not undergone peer review.
They should not be considered conclusive, used to inform clinical practice,
or referenced by the media as validated information.

Local-field-driven Scaling of Higher-order Nonlinear Susceptibilities in Plasmonic Nanocomposites With Metal Nanoparticles

Özüm Emre Aşırım

oezuem.emre.asirim@desy.de

Deutsches Elektronen-Synchrotron DESY

Research Article

Keywords: Plasmonics, Nanocomposites, Metal Nanoparticles, Nonlinear Optics, Plasmon resonance, Susceptibility

Posted Date: May 11th, 2026

DOI: https://doi.org/10.21203/rs.3.rs-9402084/v1

License: This work is licensed under a Creative Commons Attribution 4.0 International License.
Read Full License

Additional Declarations: No competing interests reported.

LOCAL-FIELD-DRIVEN SCALING OF HIGHER-ORDER NONLINEAR SUSCEPTIBILITIES IN PLASMONIC NANOCOMPOSITES WITH METAL NANOPARTICLES

Özüm Emre Aşırım*[1,2]

[1]Deutsches Elektronen-Synchrotron, Notkestraße 85, 22607 Hamburg, Germany; oezuem.emre.asirim@desy.de

[2]HAW Hamburg, Department of Computer Science, Berliner Tor 5, 20099 Hamburg, Germany; oezum.asirim@haw-hamburg.de

Abstract: We present an efficient computational framework for estimating second-, third-, and higher-order nonlinear electrical susceptibilities in plasmonic nanocomposites composed of metal–nanoparticle (MNP) matrices. Full-wave electromagnetic simulations of such systems are notoriously complex and computationally expensive, while experimental characterization is labor-intensive and resource-demanding. Our reduced-order electromagnetic model—grounded in localized surface plasmon resonance theory and nonlinear perturbation analysis—captures a highly accurate estimate of the plasmonic response with a fraction of the cost and effort. By identifying nanoparticle concentration as the principal driver of electric energy enhancement, the framework elucidates how nonlinear susceptibilities vary with key parameters such as MNP loading and polarization damping rate, enabling rapid parameter optimization. Validation against both the analytical formula for the third order susceptibility and the semi-empirical formula derived for MNP-based nanocomposites confirms the method's reliability. With its combination of physical fidelity, computational efficiency, and broad applicability, this framework provides a powerful tool for the rapid prototyping, design, and optimization of MNP based plasmonic nanocomposites for applications including high-harmonic generation and ultrafast optical switching. This work narrows the gap between computational speed and physical accuracy, advancing the rational design of MNP-based plasmonic nanocomposites.

Keywords: Plasmonics; Nanocomposites; Metal Nanoparticles; Nonlinear Optics; Plasmon resonance; Susceptibility

1. Introduction

Accurate prediction of higher-order nonlinear susceptibilities (χ_n) in plasmonic nanocomposites remains a persistent challenge. Full-wave electromagnetic simulations, such as finite-difference time-domain (FDTD) methods, require nanometer-scale spatial discretization and attosecond time steps to resolve Localized Surface Plasmon Resonance (LSPR) dynamics, leading to runtimes of days per geometry, while experimental characterization demands complex setups (Z-scan, EFISHG) and is inherently labor-intensive. These constraints limit rapid design iteration and large-scale exploration of composition–geometry–performance relationships in nonlinear nanophotonics. Several recent attempts have sought to address these bottlenecks, such as semi-analytical retrieval of second and third order susceptibilities from linear spectra in nanoparticle composites [1,2], perturbative harmonic yield models for plasmonic meta-surfaces [3-6], and phenomenological scaling approaches for higher-order susceptibilities [7-10], but very few of them explicitly offer a general framework for higher-order susceptibilities beyond χ_5.

Nonlinear plasmonics leverages the ability of metal–dielectric nanostructures to confine electromagnetic fields into deeply subwavelength volumes, enabling intrinsically weak processes such as second and third-harmonic generation, higher-order wave mixing, multiphoton photoluminescence, and ultrafast all-optical switching to occur with efficiencies far exceeding those of bulk media [4–6]. LSPRs in metallic nanoparticles (NPs) provide femtosecond-scale temporal response and nanometer-scale spatial confinement [7,8], enabling enhancement factors that can reach several orders of magnitude. Pioneering studies on metal NPs and associated plasmonic composites suggest dramatic gains in harmonic yields under resonant excitation, establishing metal–NP-based composites as promising candidates for chip-scale nonlinear photonic devices [9-12]. In such composites (Figures 1-2), control over NP size, shape, and spatial distribution enables fine-tuning of the nonlinear response. Effective-medium theories, including the Maxwell–Garnett model, have long provided analytic descriptions of composite linear permittivity and local-field factors as functions of NP volume fraction [9,10]. Dipolar spectral extensions capture third-order susceptibilities in the quasistatic limit, while interparticle coupling, symmetry breaking, and multipolar interactions extend the range of accessible nonlinearities [11,12]. Additional recent works have extended these ideas toward meta-surface-enhanced

Second Harmonic Generation (SHG) and Epsilon-Near-Zero (ENZ)-assisted nonlinear meta-structures [13,14], but their scope remains limited to specific nonlinear orders or material classes. Hence, despite the conceptual maturity, quantitative prediction of χ_4 and higher order susceptibilities remains largely intractable without resorting to high-cost numerical solvers and intricate experimental procedures, especially when extensive parameter optimization is necessary to attain the strongest nonlinear material response within a certain optical bandwidth [15-17].

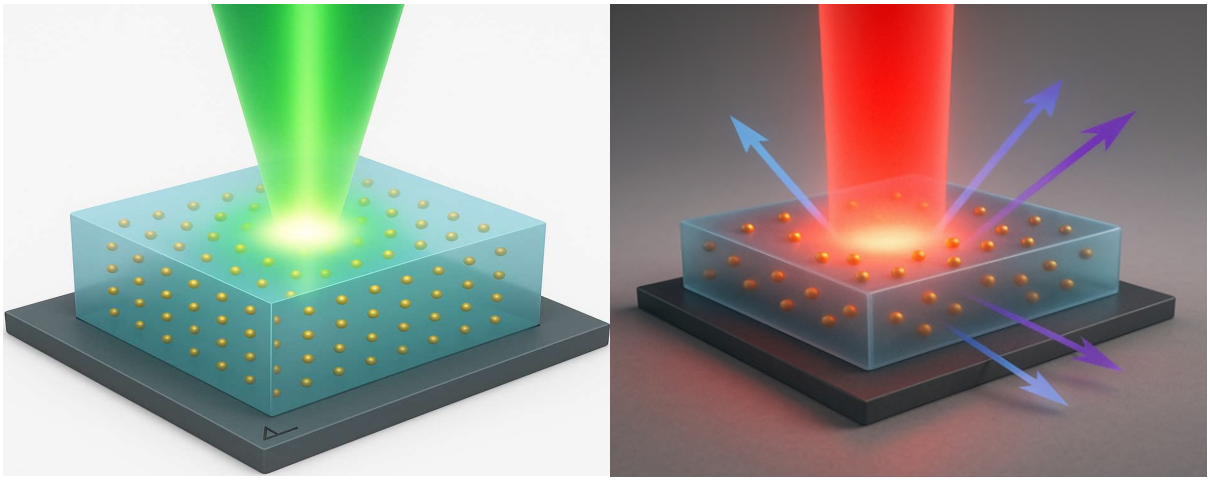


Fig. 1. 3D plasmonic nanocomposite based on metal NP-matrix structure under focused laser illumination (left). 3D plasmonic nanocomposite based on disordered metal NPs under focused laser illumination (right).

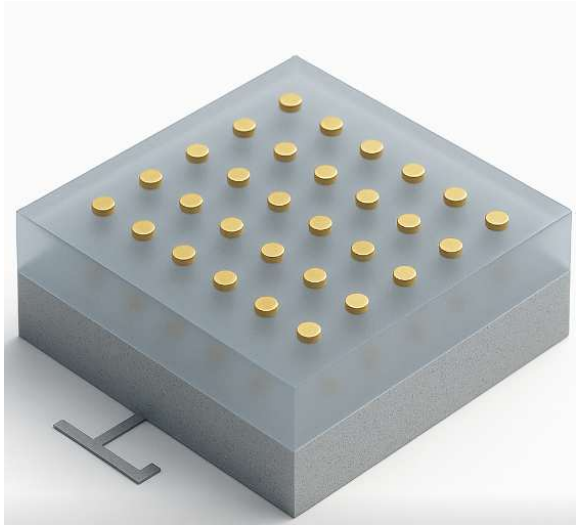


Fig. 2. 2D plasmonic metamaterial sheet based on metal NP-matrix structure.

It is important to note that while bulk centrosymmetric metals nominally suppress even-order susceptibilities, plasmonic nanocomposites unavoidably generate strong effective even-order nonlinearities because inversion symmetry is intrinsically broken at the metal–dielectric interfaces, and plasmon resonance amplifies these contributions by orders of magnitude [6,8]. This is one of the reasons why plasmonic nanocomposites are increasingly utilized in nonlinear optics. Notably, certain plasmonic materials, such as transition metal nitrides and transparent conducting oxides in their ENZ regime, have shown exceptional nonlinear performance and improved thermal stability [10–14], but their full understanding depends on computationally intensive modelling for quantitative $\chi^{(n)}$ extraction [16-18]. Semi-analytical approaches exist for $\chi^{(2)}$ and $\chi^{(3)}$ estimation from linear spectra under simplifying assumptions [16,18], but these have not been generalized to arbitrary orders or to complex NP composite architectures.

Here, we introduce an efficient, energy-based reduced-order computational framework capable of extracting second, third, and higher-order nonlinear susceptibilities ($\chi^{(2)}$ through $\chi^{(n)}$) in metal–NP matrix plasmonic nanocomposites. The model combines (i) closed-form permittivity expressions for NP and host media, derived from free and bound-electron plasma parameters [18,19], (ii) local-field enhancement factors at LSPR frequencies [18-21], and (iii) total electric energy density in the nanocomposite, to compute $\chi^{(n)}$ directly from a small set of drive-intensity sweeps [16,19,20]. This method bypasses the need for high-resolution FDTD simulations while achieving agreement with analytical and experimental benchmarks to within measurement uncertainty. By uniting physical fidelity with computational efficiency, the framework enables real-time susceptibility mapping across material compositions, geometries, and damping regimes. This capability opens new pathways for the rapid prototyping, optimization, and deployment of nonlinear photonic devices, including harmonic generators, ultrafast switches, and label-free biosensors, thereby accelerating the translation of plasmonic nanocomposites from concept to application.

2. Theory

In this section, we lay out the theoretical foundations of our reduced-order framework for extracting higher-order nonlinear susceptibilities from dielectric materials embedded with a metal NP matrix. We begin by examining the frequency-dependent permittivities of both the metal nanoparticles and the host dielectric via Drude–Lorentz models for free and bound charge carriers. These constituent permittivities are then combined through the Maxwell–Garnett mixing rule to yield an effective spectral response for the composite medium. Next, we quantify the localized field enhancement inside each nanoparticle—driven by resonant excitation of its dipolar plasmon mode—and use this to compute both the individual nanoparticle polarizability and the equivalent macroscopic field in the composite medium. Finally, by equating the total electric energy stored in the ensemble of nanoparticles, to its expansion in powers of the effective field magnitude at many distinct drive intensities, we obtain a closed linear system whose solution directly yields the second through n-th order susceptibilities of the investigated metal NP based plasmonic nanocomposite.

We start our implementation by computing the permittivities of the nanoparticles and the dielectric host medium. This requires the evaluation of the plasma frequencies for free and bound electrons ω_f and ω_b which are determined based on the density of free and bound electrons N_f and N_b as follows

$$\omega_f = \sqrt{\frac{N_f e^2}{m\varepsilon_0}}, \omega_b = \sqrt{\frac{N_b e^2}{m\varepsilon_0}} \quad (1)$$

ε_0: $Free\ space\ permittivity,\ e$: $Unit\ charge,\ m$: $Electron\ mass$

Given the angular frequency ω and the dielectric resonance frequency of the host medium ω_0, based on the polarization damping rate in the nanoparticles γ_m, and the polarization damping rate in the dielectric host medium γ_b, the metal nanoparticle and dielectric host permittivites ($\varepsilon_m, \varepsilon_d$) are evaluated as [7]

$$\varepsilon_m(\omega) = \varepsilon_0\left(1 - \frac{{\omega_f}^2}{\omega^2 - i\gamma_m\omega}\right), \qquad \varepsilon_d(\omega) = \varepsilon_0\left(\varepsilon_{background} - \frac{{\omega_b}^2}{\omega^2 - {\omega_0}^2 - i\gamma_b\omega}\right) \quad (2)$$

ω_0: $Dielectric\ resonance\ frequency\ of\ the\ host\ medium$

γ_b: $Polarization\ damping\ rate\ for\ bound\ electrons,\ \omega$: $Angular\ frequency$

γ_m: $Polarization\ damping\ rate\ for\ free\ electrons,\ \varepsilon_{background}$: $Background\ host\ permittivity,$

We first need to derive the electric field intensity that excites the metal NPs within the host medium. Given that the original source-laser electric field intensity is given as $E_s(\omega)$, only a portion of this field intensity will actually be transmitted inside the composite material. To obtain the transmitted electric field intensity at the boundary of the plasmonic nanocomposite, we need to derive the reflection coefficient between the dielectric host medium and the medium of excitation (air). This is given as

$$\Gamma(\omega) = \frac{\sqrt{\varepsilon_0} - \sqrt{\varepsilon_d(\omega)}}{\sqrt{\varepsilon_0} + \sqrt{\varepsilon_d(\omega)}} \quad (3)$$

Hence, assuming that losses are small, and the transmitted field intensity remains nearly constant inside the nanoscale composite material, which is often the case for lower nanoparticle concentrations, the drive field intensity that excites the metal NPs is found as [7]

$$E_0(\omega) = E_s(\omega)\big(1 + \Gamma(\omega)\big) = E_s(\omega)\frac{2\sqrt{\varepsilon_0}}{\sqrt{\varepsilon_0} + \sqrt{\varepsilon_d(\omega)}} \quad (4)$$

Followingly, based on the concentration of the metal nanoparticles inside the dielectric host medium, we compute the linear effective permittivity of the equivalent composite medium (Figure 3) using the Maxwell Garnett mixing rule considering the volume ratio of the metal nanoparticles (Δ) and the dielectric host medium ($1 - \Delta$) [9,10],

$$\varepsilon_{eff}(\omega) = \varepsilon_d(\omega)\left(\frac{2(1-\Delta)\varepsilon_d(\omega) + (1+2\Delta)\varepsilon_m(\omega)}{(2+\Delta)\varepsilon_d(\omega) + (1-\Delta)\varepsilon_m(\omega)}\right) = \varepsilon_0\left(1 + \chi_{eff}(\omega)\right) \quad (5)$$

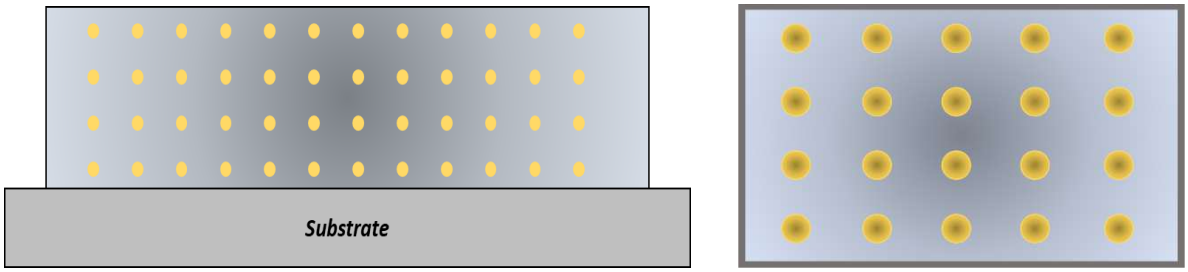


Fig. 3. Side view of a plasmonic nanocomposite based on a metal NP matrix stacked on a substrate (left), and the corresponding top view (right).

In response to the intra-material drive field $E_0(\omega)$, an enhanced electric field $E_i(\omega)$ arises inside the metal NPs due to localized surface plasmons (LSPs) [22-25]. This enhanced field intensity is dependent on the magnitude of the drive field, and the permittivites of the metal NPs and the dielectric host medium, which is given as [7]

$$E_i(\omega) = \frac{3\varepsilon_d(\omega)}{\varepsilon_m(\omega) + 2\varepsilon_d(\omega)}E_0(\omega) \quad (6)$$

Although one can evaluate the field inside the metal NPs (E_i) at every frequency, our main interest in this investigation is to find out what happens at the plasmon-resonance frequency Ω where nonlinear interactions are many orders of magnitude stronger than other parts of the spectrum [26,27]. The plasmon-resonance frequency is the frequency where the internal electric field within the metal NPs is maximized [28,29],

$$\Omega = argmax_\omega\big(E_i(\omega)\big) = argmax_\omega\left(\frac{3\varepsilon_d(\omega)}{\varepsilon_m(\omega) + 2\varepsilon_d(\omega)}E_0(\omega)\right) \quad (7)$$

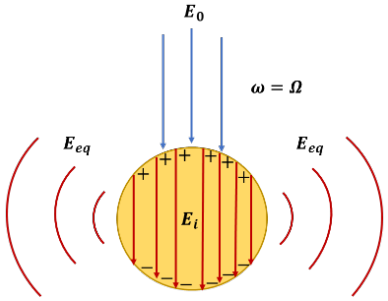


Fig. 4. Plasmonic excitation of a metal NP by a drive field E_0 and the resulting radiation of an equivalent near field.

and regarding this plasmonic field enhancement, extracting $\chi_{1,2,\dots,n}$ at $\omega = \Omega$ is naturally the main target concerning the achievement of a stronger nonlinear response that would be much more useful for the most interesting applications in nonlinear photonics. Here, we are assuming that the transmitted field intensity will remain nearly constant throughout the direction of propagation in the material, which is quite realistic as the longitudinal length or thickness of plasmonic nanocomposites is often very small (less than 1μm). Furthermore, even if the thickness would be much longer than a few micrometers, since the metal NPs usually constitute a very small volumetric portion of the host medium (in this study, the total volumetric ratio of the metal NPs is limited to 10% for realism), both the scattering loss and the conduction loss in the equivalent plasmonic nanocomposite are quite low [7-10, 30-32], ensuring constant field magnitude throughout. Nevertheless, for generalization, the validity of our algorithm is enforced by the following intra-material overall loss condition (Equation 12),

$$\alpha_s(\Omega) = -4M\pi a^2 Im\left\{\frac{\varepsilon_m(\Omega) - \varepsilon_d(\Omega)}{\varepsilon_m(\Omega) + 2\varepsilon_d(\Omega)}\right\}\left(2\pi\frac{a}{\lambda}\right) \quad (8)$$

$$\alpha_c(\Omega) = \Omega\sqrt{\frac{\mu_0\varepsilon_{eff}(\Omega)}{2}}\left[\sqrt{1 + \left(\frac{\sigma_{eff}(\Omega)}{\Omega\varepsilon_{eff}(\Omega)}\right)^2} - 1\right]^{1/2} \quad (9)$$

$$\alpha_d(\Omega) = \Omega\sqrt{\frac{\mu_0}{2}\left(\sqrt{Re\left(\varepsilon_{eff}(\Omega)\right)^2 + Im\left(\varepsilon_{eff}(\Omega)\right)^2} - Re\left(\varepsilon_{eff}(\Omega)\right)\right)} \quad (10)$$

$$\alpha_{total}(\Omega) = \alpha_s(\Omega) + \alpha_c(\Omega) + \alpha_d(\Omega), \qquad \lambda: Wavelength, \qquad c: Speed\ of\ light \quad (11)$$

$$exp(-[\alpha_s(\Omega) + \alpha_c(\Omega) + \alpha_d(\Omega)]L_m) > 0.9 \quad (12)$$

$$\alpha_s: Scattering\ loss\ coefficient, \alpha_c: Conduction\ loss\ coefficient, \alpha_d: Dielecric\ loss\ coefficient$$

$$M: Number\ of\ metal\ NPs, a: NP\ radius, \lambda: Wavelength, c: Speed\ of\ light, \mu_0: Free\ space\ permeability$$

$$L_m: Thickness\ of\ the\ plasmonic\ nanocomposite\ along\ the\ direction\ of\ propagation$$

$$\sigma_{eff}: Effective\ conductivity$$

This condition ensures that not more than 10% of the intra-material field intensity is lost, and that the assumption of a constant electric field amplitude throughout the direction of propagation in the plasmonic nanocomposite is realistic [7]. Notice that to evaluate the conduction loss coefficient α_c, the effective conductivity (σ_{eff}) of the equivalent medium has to be evaluated, which is obtained through Bruggemann's formula [33].

$$\Delta\frac{\sigma_m - \sigma_{eff}}{\sigma_m + 2\sigma_{eff}} + (1 - \Delta)\frac{\sigma_d - \sigma_{eff}}{\sigma_d + 2\sigma_{eff}} = 0 \quad (13)$$

$$\sigma_m: Conductivity\ of\ metal\ NPs, \sigma_d: Conductivity\ of\ the\ host\ medium$$

When Equation 12 is satisfied, we proceed to the next step of our framework. As one can easily notice, the enhanced electric field is maximized when $\varepsilon_m(\omega) = -2\varepsilon_d(\omega)$, which theoretically yields an infinitely enhanced field intensity, although this is not the case in practice due to the presence of polarization damping and the resulting fact that these terms have imaginary parts and are complex in nature. Therefore, for invoking a strong nonlinear material response, one should search for the drive frequency $\omega = \Omega$ where the internal field is maximized, either via a simple search algorithm or through a direct sweep of the angular frequency. This will also maximize the polarizability p of the metal nanospheres [9,34-37], from which the equivalent electric field inside the effective medium can be determined [9,37],

$$p(\Omega) = 4\pi a^3 \frac{\varepsilon_m(\Omega) - \varepsilon_d(\Omega)}{\varepsilon_m(\Omega) + 2\varepsilon_d(\Omega)}, \qquad a: Radius\ of\ the\ metal\ nanoparticles \qquad (14)$$

$$E_{eq}(\Omega) = \left(1 + \frac{M}{V}\frac{p(\Omega)}{3}\right) E_0(\Omega), \quad E_{eq}: Equivalent\ electric\ field\ in\ the\ composite\ medium \qquad (15)$$

$$M: Number\ of metal\ NPs\ in\ the\ composite\ medium, \qquad V: Volume\ of\ the\ host\ medium \qquad (16)$$

Once the equivalent electric field is known, one can move on to determine the equivalent higher order susceptibilities of the composite medium using the total energy in the medium [35,36]. The total energy in a medium is given as the sum of the electric and magnetic energies. Since the electric energy is much greater than the magnetic energy in a plasmonically excited non-magnetic medium [7,37], it is safe to assume that the total energy is equal to the electric energy. In our case, since there are M nanoparticles in the metal NP matrix, and the field intensity in the NPs is much larger than the field intensity in the dielectric host medium, under the assumption that all nanoparticles are nearly identical, the total electric energy in the medium is approximately given as [7,37]

$$W_{total}(\Omega) \approx \frac{1}{4} M \left\{ \frac{\partial\left(\omega \varepsilon'_m(\omega)\right)}{\partial \omega}\bigg|_{\omega=\Omega} \right\} |E_i(\Omega)|^2 V_{np} \quad (since\ \ E_i \gg E_0) \qquad (17)$$

$$where,\ \ \varepsilon_m(\omega) = Re\{\varepsilon_m(\omega)\} + iIm\{\varepsilon_m(\omega)\} = \varepsilon'_m(\omega) + i\varepsilon''_m(\omega)$$

Due to the fact that strong nonlinear interactions will occur in the composite medium as a result of the high equivalent field intensity originated by the totality of the LSPRs (E_{eq}) [38], the total equivalent electric energy density in the medium can also be expressed as [7,35,37,38],

$$\frac{1}{4} M V_{np} \left\{ \frac{\partial\left(\omega \varepsilon'_m(\omega)\right)}{\partial \omega}\bigg|_{\omega=\Omega} \right\} |E_i|^2 = V \left\{ \frac{1}{4} \left\{ \frac{\partial\left(\omega \varepsilon'_{eff}(\omega)\right)}{\partial \omega}\bigg|_{\omega=\Omega} \right\} \left|E_{eq}\right|^2 + \varepsilon_0 \sum_{j=2}^{n} \frac{\chi^{(j)}(\Omega)\left|E_{eq}\right|^{j+1}}{j+1} \right\} \qquad (18)$$

since,

$$w(E) = \int_0^E D(E')\, dE', \quad D = \varepsilon_0 E_{eq} + P_{lin} + \varepsilon_0 \sum_{n=2}^{\infty} \chi^{(n)} {E_{eq}}^{n+1},\ w_{lin}(\Omega) = \frac{1}{4} \left\{ \frac{d\{\omega Re[\varepsilon(\omega)]\}}{d\omega}\bigg|_{\omega=\Omega} \right\} |E(\Omega)|^2 \quad (19)$$

$$w: Electric\ energy\ density, D: Electric\ flux\ density,\ w_{lin}/P_{lin}: Linear\ electric\ flux/polarization\ density$$

This formulation adopts a time-averaged energy-based expansion, and naturally yields an effective nonlinear susceptibility, representing the aggregate response without resolving individual frequency-mixing pathways.

Here, things get slightly tricky. To evaluate the (n-1) higher order susceptibilities $\{\chi_2, \chi_3, ..., \chi_n\}$, we need (n-1) independent equations. The only way to obtain such an equation system is to excite the composite plasmonic medium via (n-1) slightly different drive field intensities $\{E_{0,1}, E_{0,2}, \ldots, E_{0,n-1}\}$ which will yield different enhanced fields $\{E_{i,1}, E_{i,2}, \ldots, E_{i,n-1}\}$ and different equivalent field intensities $\{E_{eq,1}, E_{eq,2}, \ldots, E_{eq,n-1}\}$. Here, it is recommended to choose the drive field intensities to be only slightly different from each other, and between $10^6 V/m$ and $10^8 V/m$ regarding practical values [7,37-39]. The degree of difference between subsequent drive intensities depends on the maximum susceptibility order to keep the matrix well-conditioned, but a factor between 1.01 and 1.1 works well up to a susceptibility order of 12. Making use of the resulting aggregated equation system based on (n-1) drive field excitations with slightly different intensities ($E_{0,k}$), one can solve for the higher order suceptibilities as follows:

First, the electric field in the metal NPs, and the resulting equivalent electric field in the plasmonic nanocomposite is evaluated for each drive intensity $E_{0,k}$

$$E_{i,k}(\Omega) = \frac{3\varepsilon_d(\Omega)}{\varepsilon_m(\Omega) + 2\varepsilon_d(\Omega)} E_{0,k}(\Omega), \qquad E_{eq,k}(\Omega) = \left(1 + \frac{M}{V}\frac{p(\Omega)}{3}\right) E_{0,k}(\Omega), \qquad k = 1, \ldots, n-1 \quad (20)$$

then, the electric energy equivalence is registered for each drive intensity $E_{0,k}(\Omega)$, forming a system of equations,

$$W_{total,k} = \frac{1}{4} M V_{np} \left\{ \frac{\partial\left(\omega \varepsilon'_m(\omega)\right)}{\partial \omega}\bigg|_{\omega=\Omega} \right\} \left|E_{i,k}\right|^2$$
$$= V \left\{ \frac{1}{4} \left\{ \frac{\partial\left(\omega \varepsilon'_{eff}(\omega)\right)}{\partial \omega}\bigg|_{\omega=\Omega} \right\} \left|E_{eq,k}\right|^2 + \varepsilon_0 \sum_{j=2}^{n} \frac{\chi^{(j)}(\Omega) \left|E_{eq,k}\right|^{j+1}}{j+1} \right\} \quad (21)$$

here, the elements of the kth row of the coefficient matrix can be determined as, $c_{j-1,k} = \varepsilon_0 V \frac{|E_{eq,k}|^{j+1}}{j+1}$, therefore, the higher order susceptibilities can be evaluated based on the system of linear equations given in Equation 22, which is solved as given in Equation 23,

$$\begin{bmatrix} W_{total,1}(\Omega) - V\frac{1}{4}\left\{ \frac{\partial\left(\omega \varepsilon'_{eff}(\omega)\right)}{\partial \omega}\Big|_{\omega=\Omega} \right\} \left|E_{eq,1}\right|^2 \\ W_{total,2}(\Omega) - V\frac{1}{4}\left\{ \frac{\partial\left(\omega \varepsilon'_{eff}(\omega)\right)}{\partial \omega}\Big|_{\omega=\Omega} \right\} \left|E_{eq,2}\right|^2 \\ . \\ W_{total,n-1}(\Omega) - V\frac{1}{4}\left\{ \frac{\partial\left(\omega \varepsilon'_{eff}(\omega)\right)}{\partial \omega}\Big|_{\omega=\Omega} \right\} \left|E_{eq,n-1}\right|^2 \end{bmatrix} = \begin{bmatrix} c_{11} & c_{12} & . & c_{1,n-1} \\ c_{21} & c_{22} & . & c_{2,n-1} \\ . & . & . & . \\ c_{n-1,1} & c_{n-1,2} & . & c_{n-1,n-1} \end{bmatrix} \begin{bmatrix} \chi_2(\Omega) \\ \chi_3(\Omega) \\ . \\ \chi_n(\Omega) \end{bmatrix} \quad (22)$$

$$\begin{bmatrix} \chi_2(\Omega) \\ \chi_3(\Omega) \\ . \\ \chi_n(\Omega) \end{bmatrix} = \begin{bmatrix} c_{11} & c_{12} & . & c_{1,n-1} \\ c_{21} & c_{22} & . & c_{2,n-1} \\ . & . & . & . \\ c_{n-1,1} & c_{n-1,2} & . & c_{n-1,n-1} \end{bmatrix}^{-1} \begin{bmatrix} W_{total,1}(\Omega) - V\frac{1}{4}\left\{ \frac{\partial\left(\omega \varepsilon'_{eff}(\omega)\right)}{\partial \omega}\Big|_{\omega=\Omega} \right\} \left|E_{eq,1}\right|^2 \\ W_{total,2}(\Omega) - V\frac{1}{4}\left\{ \frac{\partial\left(\omega \varepsilon'_{eff}(\omega)\right)}{\partial \omega}\Big|_{\omega=\Omega} \right\} \left|E_{eq,2}\right|^2 \\ . \\ W_{total,n-1}(\Omega) - V\frac{1}{4}\left\{ \frac{\partial\left(\omega \varepsilon'_{eff}(\omega)\right)}{\partial \omega}\Big|_{\omega=\Omega} \right\} \left|E_{eq,n-1}\right|^2 \end{bmatrix} \quad (23)$$

To mitigate ill-conditioning in the polynomial inversion of nonlinear susceptibilities, the driving field amplitudes should be sufficiently separated—e.g., logarithmically spaced—thereby improving the conditioning of the resulting Vandermonde system and enhancing robustness against numerical noise. To keep things traceable and compact, the entire procedure is summarized in Table 1 as a pseudocode. The formulation should be interpreted as an effective parameter extraction framework. The derived susceptibilities represent macroscopic, design-relevant quantities rather than fundamental nonlinear coefficients. The approach is most valid in the dilute, weak-coupling regime and is intended for rapid trend prediction rather than exact quantitative accuracy.

Table 1. Pseudocode for the outlined procedure for extracting higher-order susceptibilities

Algorithm — Higher-order susceptibility extraction for metal-NP matrices in a dielectric host medium

1) Constituent permittivities (Drude–Lorentz):
Compute $\varepsilon_m(\omega)$ and $\varepsilon_d(\omega)$ from the given free/bound-electron parameters.

2) Interface transmission (air → host) and drive inside composite:
$n_h(\omega) = \sqrt{\varepsilon_d(\omega)}$; $t(\omega) = 2 / (1 + n_h(\omega))$ (normal incidence);
$E0(\omega) = |t(\omega)| \cdot E_{inc}(\omega)$.

3) Maxwell–Garnett effective permittivity (dilute, spheres):
$\varepsilon_{eff}(\omega) = \varepsilon_d \cdot [\, \varepsilon_m + 2\varepsilon_d + 2\Delta(\varepsilon_m - \varepsilon_d) \,] / [\, \varepsilon_m + 2\varepsilon_d - \Delta(\varepsilon_m - \varepsilon_d) \,]$.

4) Internal NP field and LSPR search:
$L(\omega) = 3\varepsilon_d / (\varepsilon_m(\omega) + 2\varepsilon_d)$; $E_i(\omega) = |L(\omega)| \cdot E0(\omega)$.
Find $\Omega = \operatorname{argmax}_{\omega \in [\omega_{min}, \omega_{max}]} E_i(\omega)$ (coarse sweep on a dense grid, then golden-section refine).

5) Loss gate at Ω (proceed only if transmission is high):
From $\varepsilon_{eff}(\Omega)$ (and modeled scattering/coupling), get $\alpha_d(\Omega)$, $\alpha_s(\Omega)$, $\alpha_c(\Omega)$.
If $\exp(-[\alpha_s+\alpha_c+\alpha_d] \cdot L_m) \le 0.9$ → adjust Δ, L_m, or γ and repeat 1–5.

6) Polarizability and number density at Ω:
$p(\Omega) = 3\varepsilon_0 \varepsilon_d V_{np} \cdot (\varepsilon_m(\Omega) - \varepsilon_d) / (\varepsilon_m(\Omega) + 2\varepsilon_d)$.
$\rho = M / V$ ($\simeq \Delta / V_{np}$ in dilute limit).

7) Macroscopic equivalent field (Lorentz/Clausius–Mossotti at Ω):
For J drives near Ω (geometric spacing; $J \ge$ #orders+2):
$E_{eq}^{(j)} = |1 + \rho \cdot p(\Omega)/3| \cdot E0^{(j)}$, $E_i^{(j)} = |L(\Omega)| \cdot E0^{(j)}$.

8) Brillouin linear-energy factors at Ω (central difference on $g(\omega)=\omega \cdot Re\{\varepsilon(\omega)\}$):
$D_m = d/d\omega[\, \omega \cdot Re\{\varepsilon_m(\omega)\} \,]|_{\Omega}$;
$D_{eff} = d/d\omega[\, \omega \cdot Re\{\varepsilon_{eff}(\omega)\} \,]|_{\Omega}$.

9) Energy balance per drive and linear system assembly:
For each $j = 1..J$:
$U_{NP}^{(j)} = (1/4) \cdot M \cdot V_{np} \cdot D_m \cdot |E_i^{(j)}|^2$
$U_{lin}^{(j)} = (1/4) \cdot V \cdot D_{eff} \cdot |E_{eq}^{(j)}|^2$
$b_j = U_{NP}^{(j)} - U_{lin}^{(j)}$
For each even k in $K = \{2,4,\ldots,n_{max}\}$:
$C_{j,k} = \varepsilon_0 \cdot [1/(k+1)] \cdot |E_{eq}^{(j)}|^{(k+1)}$

10) Solve for susceptibilities at Ω:
Find $\hat{\chi} = \operatorname{argmin}_{\chi \ge 0} \|C\chi - b\|_2^2$ (nonnegative least squares or mild Tikhonov-regularized normal equations);
Output $\{ |\chi^{(k)}(\Omega)| \}_{k \in K}$, Ω, and residual $\|C\hat{\chi} - b\|_2$.

3. Parameters of the Simulation

The simulations are carried out for the commonly used plasmonic nanocomposite consisting of silver (Ag) nanoparticles embedded in a titanium dioxide (TiO_2) host. The optical response of the metallic inclusions are described using a Drude–Lorentz formulation with a plasma frequency of $\omega_p = 1.37 \times 10^{16}\text{rad/s}$, and a high-frequency relative permittivity of $\varepsilon_\infty = 1$. The bound-electron polarization damping rate of the host medium is taken as $\gamma_b = 10^{12}\text{Hz}$, and its background relative permittivity ($\varepsilon_{\text{background}}$) is roughly equal to 6.25, corresponding to a refractive index of approximately 2.5 in the IR-VIS-UV regime, which is in agreement with the spectroscopy measurements for TiO_2. The dielectric resonance frequency of the host is set at its experimentally observed value $f_0 \approx 750\text{THz}$, and all calculations are performed for optical frequencies in the range $100\text{THz} < f < 1500\text{THz}$, within which the plasmon resonance frequency is searched for and located. For a TiO_2 host embedded with silver nanoparticles, the plasmon resonance frequency is located between 500THz and 700THz for diluted NP embedding ($\Delta < 0.1$), and varies with Δ.

Geometric parameters of the nanocomposite are chosen to be representative of experimentally realizable samples. The nanoparticle radius is fixed at $a = 15\text{nm}$, and the nanocomposite length along the propagation direction (thickness) is set to $L_m = 300\text{nm}$, with a cross-sectional area of $A_{cs} = 1\mu\text{m}^2$. Electrical parameters are also specified explicitly (see Table 2). The conductivity of the metallic inclusions is taken as $\sigma_m = 6.3 \times 10^7\text{S/m}$, while the TiO_2 host medium is treated as insulating with $\sigma_h \sim 0\text{S/m}$. The effective composite conductivity is correspondingly estimated as $\sigma_{\text{eff}} < 10^{-4}\ \text{S/m}$ for filling fractions Δ<0.1, ensuring that the simulated system remains in the dilute, non-percolating regime.

Table 2. Simulation parameters for Silver (Ag) nanoparticles embedded in Titanium Dioxide (TiO_2)

Parameter	Symbol	Value/Range
Plasma frequency (Ag)	ω_p	$1.37 \times 10^{16} rad/s$
High-frequency permittivity (Ag)	ε_∞	1
Background host (TiO2) permittivity	$\varepsilon_{background}$	6.25
Nanoparticle radius	a	*15nm*
Thickness of the nanocomposite	L_m	*300nm*
Conductivity of metal NPs	σ_m	$6.3 \times 10^7 S/m$
Conductivity of host medium	σ_h	$\sim 0\ S/m$
Effective conductivity (composite)	σ_{eff}	$< 10^{-4}\ S/m$ $(for \Delta < 0.1)$
Angular frequency	ω	$2\pi \times (100THz < f < 1500THz)$
Dielectric angular resonance frequency (host)	ω_0	$2\pi \times 750THz$
Polarization damping (bound e⁻)	γ_b	$10^{12} Hz$
Nanoparticle volume	V_{np}	$(4\pi/3) \times a^3$
Number of nanoparticles	M	$(V \times \Delta)/V_{np}$
Nanocomposite cross-sectional area	A_{cs}	$1\mu m^2$
Nanocomposite volume	V	$A_{cs} \times L_m$

4. Results

4.1 Variation of higher-order susceptibilities with total metal composition ratio

At low metal loadings (Δ<0.01), which are common in practice due to cost and ease of fabrication, our Drude–Lorentz–based permittivity model predicts small equivalent electric field enhancement and low overall polarizability. This is because when low concentration is accounted through the Maxwell–Garnett mixing and the subsequent energy-balance procedure, the total stored energy in the nanocomposite remains small, yielding the usual lower values for all susceptibility orders, comparable to the pure host material without metal NP embeddings. As nanoparticle concentration increases, however, the total energy in the nanocomposite increases, and strong resonant coupling boosts the equivalent macroscopic field. This surge in stored electric energy drives a steep rise in every χ_n curve, reflecting the universal sensitivity of nonlinear processes to electric field strength (Figures 5-6).

Once the nanocomposite reaches a certain metal NP loading (Δ=0.1), further increases in metal fraction do not yield the same degree of enhancement. Enhanced radiative broadening and intrinsic polarization damping reshape the effective permittivity via Maxwell–Garnett mixing, reducing the equivalent electric field and the total energy stored in the plasmonic nanocomposite. In our framework, this reduction of energy translates directly into the suppression of further enhancement for all susceptibility orders. Crucially, higher-order susceptibilities, which depend on higher powers of the equivalent electric field, exhibit the most dramatic enhancements for $0 < \Delta < 0.05$, but also the most pronounced plateauing for $\Delta > 0.05$. Overall, concerning cost and fabrication challenges, the composition-dependent higher-order susceptibilities imply a clear design rule: for any target harmonic order, one should simply select the smallest nanoparticle fraction that sufficiently raises χ_n to the intended level as further enhancement via additional metal NPs is relatively lower. Here, the maximum value of Δ is limited to 0.1 as this is often the case in practice [37].

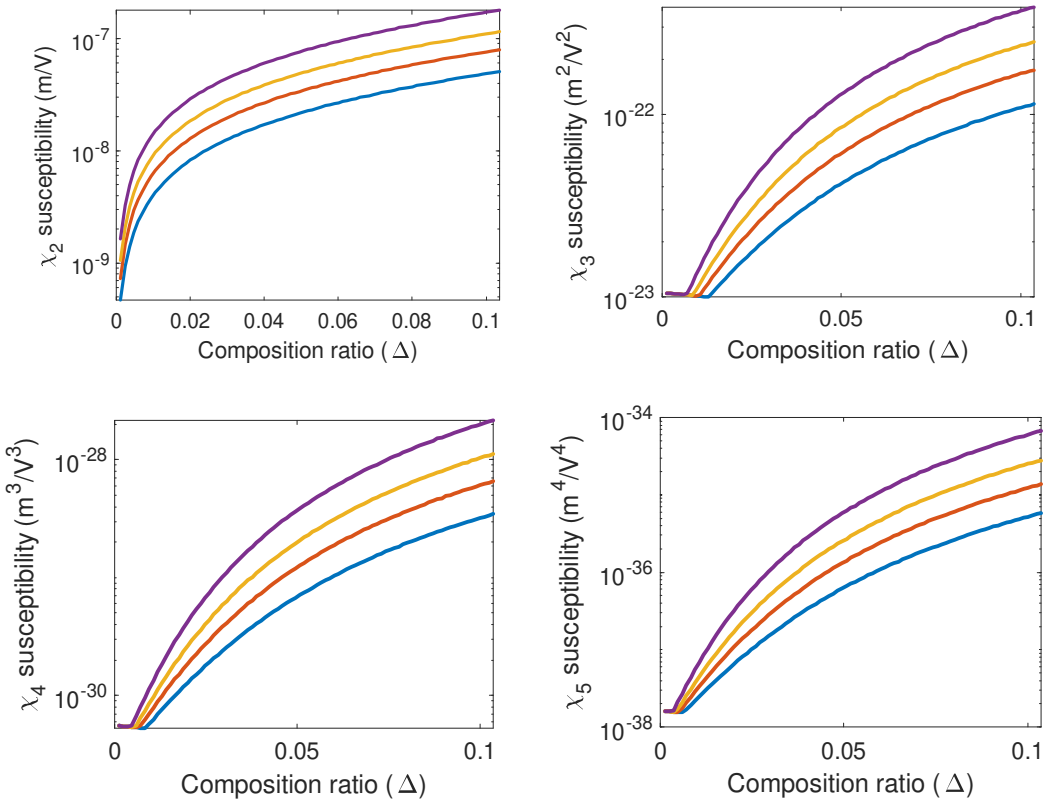


Fig. 5. Susceptibility $(\chi_2, \chi_3, \chi_4, \chi_5)$ versus composition ratio (Δ) for different metal NP polarization damping rates, corresponding to $\gamma_m = \{1 \times 10^{13} Hz, 1.5 \times 10^{13} Hz, 2 \times 10^{13} Hz, 3 \times 10^{13} Hz\}$ represented by violet, gold, orange, and blue curves respectively.

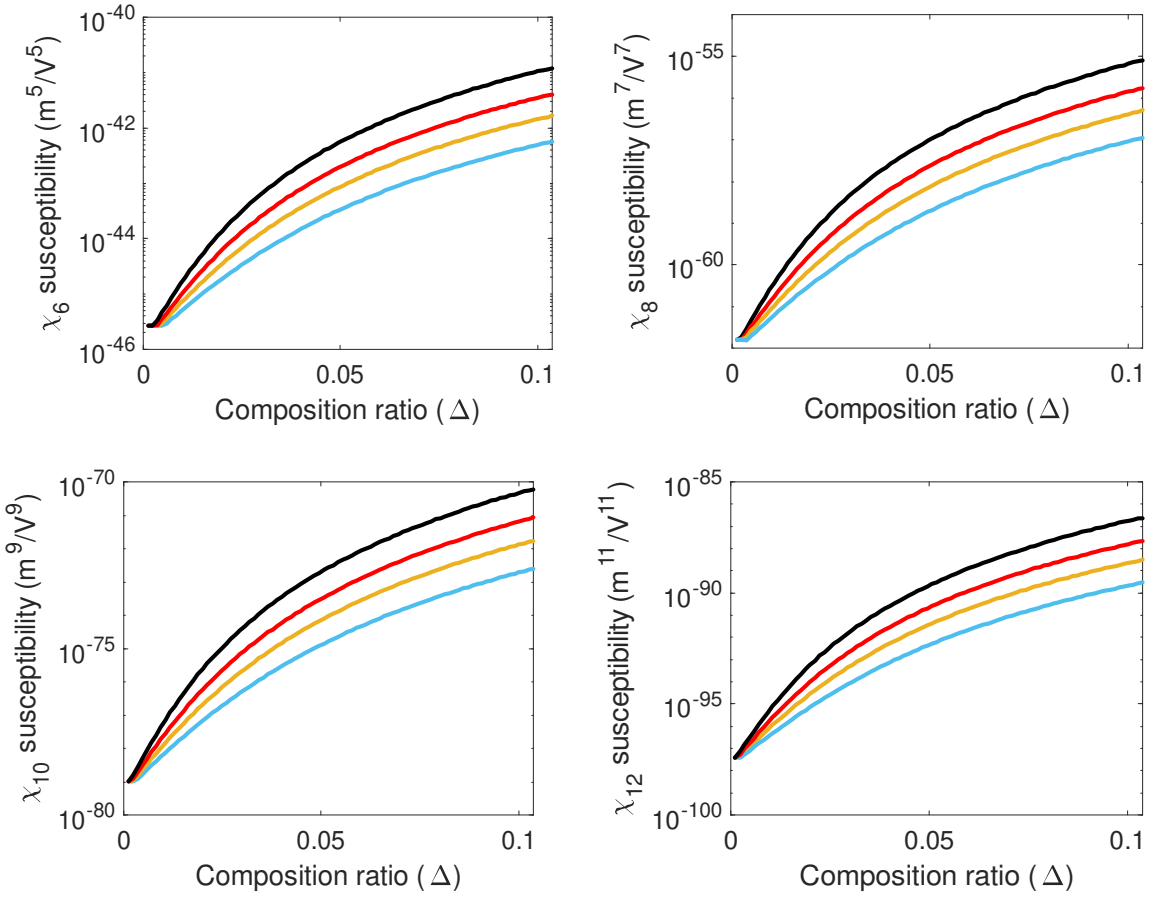


Fig. 6. Susceptibility $(\chi_6, \chi_8, \chi_{10}, \chi_{12})$ versus composition ratio (Δ) for different metal NP polarization damping rates, corresponding to $\gamma_m = \{1 \times 10^{13} Hz, 1.5 \times 10^{13} Hz, 2 \times 10^{13} Hz, 3 \times 10^{13} Hz\}$ represented by black, red, gold, and cyan curves respectively.

4.2 Variation of higher-order susceptibilities with the polarization damping rate of metal NPs

As the polarization damping rate of the metal nanoparticles ($\gamma_m = \gamma_{metal}$) increases, the resonant permittivity response becomes progressively broadened and attenuated, directly diminishing the local-field enhancement factor and nanoparticle polarizability derived from $\varepsilon_m(\omega)$. In our framework, these quantities feed into the equivalent macroscopic field, which in turn determine the total stored electric energy in the plasmonic nanocomposite. Consequently, all extracted susceptibilities (χ_n) decline steadily with increasing γ_{metal}. To put it more simply, at low damping, the sharp plasmon resonance maximizes stored energy and yields the largest χ_n values; as γ_{metal} grows, the LSPR weakens, reducing energy storage and driving every susceptibility curve downward in parallel.

Higher-order susceptibilities exhibit markedly greater sensitivity to γ_{metal} than lower orders. Because χ_n enters the energy-balance equations via being multiplied by the (n+1)-th power of the equivalent electric field magnitude, even modest reductions in field enhancement produce disproportionately large drops in extreme nonlinearities. Thus, χ_{10} and χ_{12} fall off more steeply with γ_{metal} than χ_2 or χ_3, and their optimal performance demands the lowest possible free-electron polarization damping. This hierarchy implies the critical need for high-quality, low-loss metal nanoparticles via surface passivation, alloying, or crystallinity control to sustain strong nonlinear plasmonic responses, especially for applications targeting high-order harmonic generation.

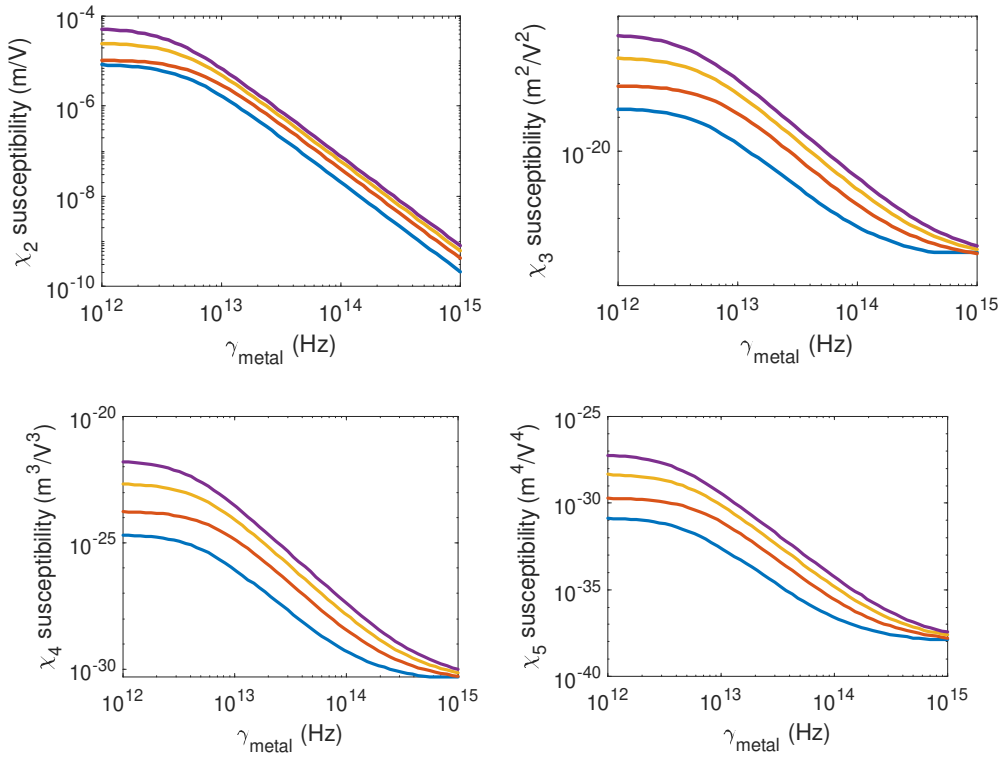


Fig. 7. Susceptibility $(\chi_2, \chi_3, \chi_4, \chi_5)$ versus metal NP polarization damping rate (γ_{metal}) for different composition ratios corresponding to $\Delta = \{0.10, 0.08, 0.06, 0.04\}$ represented by violet, gold, orange, and blue curves respectively.

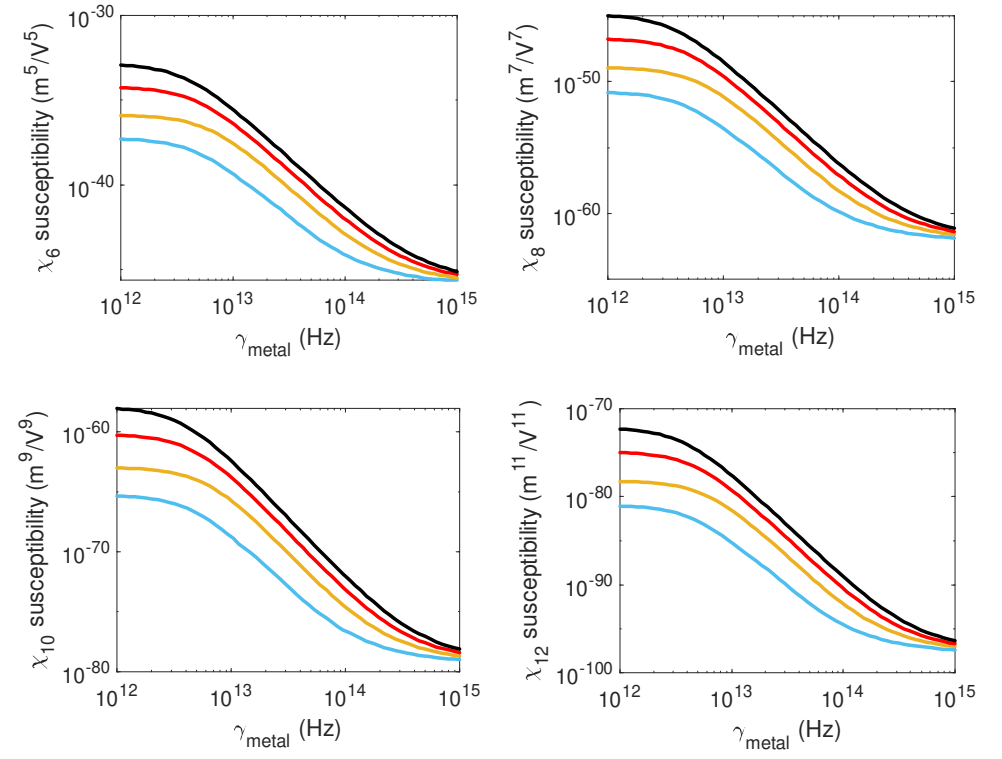


Fig. 8. Susceptibility $(\chi_6, \chi_8, \chi_{10}, \chi_{12})$ versus metal NP polarization damping rate (γ_{metal}) for different composition ratios corresponding to $\Delta = \{0.10, 0.08, 0.06, 0.04\}$ represented by black, red, gold, and cyan curves respectively.

5. Discussion and limitations of the study

The variation of susceptibilities based on composition ratio and polarization damping reveal the central role of local-electric field enhancement and energy storage in driving nonlinear response. At low nanoparticle volume fractions, the Drude–Lorentz permittivities yield only modest field concentration and therefore low χ_n values. As loading increases, the equivalent macroscopic field is amplified, which raises the stored electric energy and drives a rapid growth in all χ_n curves. However, beyond a certain loading, broadened resonance, which is captured via Maxwell–Garnett mixing, diminish the equivalent electric field enhancement, causing susceptibility plateau. This is consistent with prior effective-medium studies of χ_2 and χ_3 in dilute composites [9,10,12,30].

Comparing our energy-based predictions to full-wave simulations reveals the accuracy and efficiency of the framework. Finite-difference time-domain method can be used to compute arbitrary orders but incurs extreme computational cost—multi-day runtimes for modest three-dimensional assemblies due to nanometer spatial meshes and femtosecond timesteps [6,7] on a standard computer. Whereas our reduced-order workflow reproduces $\chi_{2,\ldots,n}$ while running in 15-17 seconds on a standard computer (11th Gen Intel(R) Core(TM) i7-11800H, 2.30GHz, 16GB RAM). This balance of physical fidelity and speed sets our method apart as a practical tool for the reliable estimation of high-order nonlinear susceptibilities.

Despite its strengths, our model relies on several simplifying assumptions that define its domain of validity. Firstly, the distribution of metal NPs is assumed to be homogenous or ordered, so this model will not work for plasmonic nanocomposites with disordered metal NPs in its current form and requires adaptation. Though, the nice thing about our model is that it is highly adaptable by design. Second, we adopt the quasistatic, dipolar approximation—appropriate for nanoparticle diameters below 50nm, and neglect magnetic energy contributions, higher multipolar modes, and nonlocal or quantum-size effects [6,17,37]. Third, the Maxwell–Garnett mixing rule presumes dilute to moderate volume fractions and spherical inclusions; deviations from these conditions (e.g., anisotropic shapes or dense packings) will introduce quantitative errors. Additionally, ensemble dispersity and substrate interactions, which can shift and broaden resonances [38,39], are also omitted, but can be incorporated by adjusting damping parameters. Finally, the assumption of constant electric field magnitude throughout the longitudinal direction of the plasmonic nanocomposite is not necessarily a limitation of our study, because the composition ratio is less than or equal to 0.1 here, and this diluted distribution mostly satisfies the constant electric-field-magnitude condition under homogenous distribution of the metal NPs. Nevertheless, our framework is applicable for many practical cases. Users of our algorithm should therefore apply the framework within these bounds, and supplement it with corrections when exploring beyond the quasistatic, monodisperse regime.

Looking forward, several extensions can enrich the framework's predictive power. Multipolar contributions can be included via generalized spectral–representation theory, capturing shape-dependent resonances beyond the dipole [7,37]. Nonlocal and quantum-size effects, critical for NPs with a diameter below 10 nm, could be modeled by coupling hydrodynamic or density-functional approaches into the permittivity expressions [4,6,17,18]. Time-dependent or pump-probe scenarios may be addressed by embedding the energy-balance formulation within a temporal evolution scheme. Finally, the method can be adapted to structured metasurfaces and hybrid photonic–electronic platforms by replacing bulk effective-medium mixing with rigorous coupled-mode or scattering-matrix formalisms. However, as an initial model, by harmonizing computational expediency with fundamental physics, our energy-based susceptibility extraction offers broad impact for both research and practical applications.

6. Model accuracy: High-order electric susceptibility versus total metal NP composition ratio

The susceptibility–composition curves obtained in this study display a progression characteristic of many metal–dielectric nanocomposite systems: a pronounced enhancement at low metal nanoparticle loading, a gradual reduction in slope at intermediate compositions, and eventual saturation as the metal fraction becomes larger. This sequence has been documented in several experimental and theoretical works on plasmonic composites [40,44-48], and is well understood in terms of plasmonic local-field enhancement, interparticle coupling, and absorption-induced damping.

To confirm the accuracy of the numerical simulation, the effective third-order nonlinear susceptibility $\chi^{(3)}$ of the metal-dielectric nanocomposite was validated against the analytical results derived from the Maxwell-Garnett Effective Medium Theory (MG-EMT). In the dilute limit, the effective nonlinearity is given by [41-43]:

$$\chi^{(3)}(\Delta) = \Delta \left| \frac{3\varepsilon_h}{\varepsilon_m + 2\varepsilon_h} \right|^4 \chi_{np}{}^{(3)} \quad (24)$$

Where ε_h is the permittivity of the host medium (in this case TiO_2), and ε_m, $\chi_{np}{}^{(3)}$ are the permittivity and intrinsic nonlinear susceptibility of the metal inclusions (nanoparticles) respectively.

The simulation data were benchmarked by comparing the computed $\chi^{(3)}(\Delta)$ for $\gamma_m = 1 \times 10^{13}$Hz across the range $\Delta \in [0, 0.1]$ against the analytical scaling predicted by the fourth-power dependence on the local field enhancement factor $f_e = \frac{3\varepsilon_h}{\varepsilon_m + 2\varepsilon_h}$. At the limit $\Delta \to 0$, the numerical model converges to the host background response, consistent with the analytical framework. In the linear regime of low volume fractions, the simulated susceptibility exhibits a monotonic growth trend that aligns with the analytical model, confirming the correct implementation of the effective medium interaction terms (Fig. 9). Deviations at higher concentrations serve as a physical indicator of the transition from the Maxwell-Garnett regime toward the percolation threshold, where higher-order coupling effects necessitate more sophisticated homogenization methods (e.g., Bruggeman EMT or full-wave electromagnetic solvers). However, as we have mentioned, $\Delta < 0.1$ is valid for most of the practical scenarios, since most high-fidelity nonlinear optical devices (like optical limiters or switches) are optimized in this dilute regime to maximize local field enhancement without inducing significant linear loss.

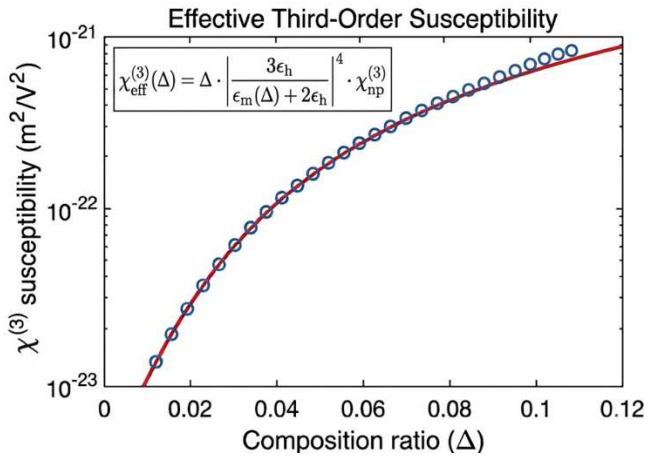


Fig. 9. Comparison of the numerical and analytical results for $\chi^{(3)}(\Delta)$. The blue dots represent numerical data, where as the red curve represents the analytical results.

Early experimental work by Ricard et al. [44] on metal colloids demonstrated a sharp rise in nonlinear optical response at low filling fractions, attributable to the formation of strong local-field factors near the localized surface plasmon resonance. Hache et al. [45] confirmed this behavior for the third-order susceptibility in small-particle systems, and reported the slower growth at intermediate composition ratios as consistent with effective-medium predictions. Markel and Shalaev [46] showed that local-field distributions lead to sublinear scaling of the nonlinear response with inclusion fraction, in close agreement with the curvature we observe beyond the initial rise. Likewise, Sarychev and Shalaev [12] demonstrated that electromagnetic field intensities in composites inherently produce saturation-like behavior at higher composition ratios due to enhanced damping, in direct agreement with the plateau observed in our calculations. In particular, Del Coso et al. [47] measured $\chi^{(3)}$ of Cu:Al_2O_3 nanocomposites and observed precisely the same three-stage progression: steep enhancement at low loading, reduced incremental gain in the mid-range, and a plateau near percolation. This graphical behavior is modeled by the stretched exponential scaling law (SESL, see Equation 25), which captures the full low–mid–high loading trajectory for describing composition-dependent nonlinearities in metal–dielectric composites [48].

In our case, Figures 5–6 present the computed n-th order susceptibilities of the plasmonic Ag - TiO_2 composite as a function of the Ag-NP composition ratio Δ, we intend to see if our simulation results obey SESL:

$$\chi^{(n)}(\Delta) = \chi^{(n)}_{min} + \left(\chi^{(n)}_{max} - \chi^{(n)}_{min}\right)\left[1 - \exp\left(-\left(\frac{\Delta}{\Delta^{(n)}_0}\right)^{\beta^{(n)}}\right)\right] \qquad (25)$$

Here, $\chi^{(n)}_{min}$ corresponds to the limiting susceptibility of the pure host (Δ→0), and $\chi^{(n)}_{max}$ corresponds to the near-saturation value at high metal loading. $\Delta^{(n)}_0$ is a characteristic composition scale indicating the onset of significant nonlinear enhancement, and $\beta^{(n)}$ is the stretching exponent describing the broadness of the transition. The fitting of all curves revealed that the curvature of $\chi^{(n)}(\Delta)$ is essentialy order-independent, allowing the use of common parameters for all n. The primary order-dependent variation arises from the amplitude term $\chi^{(n)}_{max} - \chi^{(n)}_{min}$, which reflects differences in the intrinsic nonlinear coefficients of each order. We found that our results perfectly obey SESL with well-defined fitting parameters. Table 3 summarizes the extracted parameters for all computed even-order susceptibilities obtained from the data in Figures 5–6.

Table. 3. Susceptibility order versus SESL-based fitting parameters for our simulation results

Order (n)	Units	$\chi^{(n)}_{min}$	$\chi^{(n)}_{max}$	$\beta^{(n)}$	$\Delta^{(n)}_0$
2	m/V	3×10^{-10}	1.7×10^{-7}	0.70	0.020
4	m^3/V^3	8×10^{-31}	4×10^{-28}	0.66	0.019
6	m^5/V^5	5×10^{-46}	7×10^{-42}	0.63	0.018
8	m^7/V^7	10^{-62}	10^{-55}	0.62	0.0175
10	m^9/V^9	2×10^{-79}	8×10^{-71}	0.60	0.0170
12	m^{11}/V^{11}	7×10^{-98}	3×10^{-87}	0.58	0.0165

The extracted values show that, despite a 12-order range in nonlinear susceptibilities, the composition dependence can be described by the same scaling, suggesting the consistency of our proposed algorithm.

7. Conclusion

We have presented an energy-based, reduced-order framework for the quantitative extraction of second through n-th order nonlinear susceptibilities in plasmonic nanocomposites with metal nanoparticles. By combining analytical permittivity models, Maxwell–Garnett mixing, and a compact energy-balance formulation, our method captures the essential physics of LSPR–induced field and susceptibility enhancements while reducing computational cost by orders of magnitude relative to full-wave simulations. The resulting χ_n curves display clear monotonic dependence on NP loading and metal NP polarization damping rate, offering unambiguous design rules for tuning higher-order susceptibilities. This approach enables rapid, high-fidelity exploration of composition, size, and material parameters for tuning higher-order susceptibilities within a single sweep-and-solve workflow, making it a powerful tool for both fundamental studies and practical device prototyping. The present formulation is intended as an effective, time-averaged framework that captures aggregate nonlinear response under quasistatic, weak-coupling conditions, providing reliable design-level estimates rather than frequency-resolved nonlinear dynamics. Looking ahead, extensions to multipolar resonances, time-dependent scenarios, nonlocal effects, and structured meta-surfaces promise to broaden the framework's applicability, while its compatibility with inverse-design positions it as a versatile engine for nonlinear photonic materials based on metal-NP-induced plasmonic field enhancement.

Data availability

All data that support the findings of this study are included within the article (and any supplementary files).

Code availability

The code used to support the findings of this study is available at the following link:

https://drive.google.com/file/d/10k6xetLNabYLcQg9w5U7ZcgSEK8U8xrk/view?usp=sharing

Conflict of interest: On behalf of all authors, the corresponding author states that there is no conflict of interest.

Ethics, Consent to Participate, and Consent to Publish declarations: not applicable

Funding statement: This research received no external funding.

ORCID iD

Özüm Emre Aşırım https://orcid.org/0000-0003-0531-401X

References

[1] M. Balaei and T. Naseri, "Enhancement of second-harmonic field and nonlinear dispersion via a composite of elliptical cylinder nanoparticles," Journal of Applied Physics, vol. 134, no. 11, p. 113101, Sep. 2023, doi: 10.1063/5.0167860.

[2] T. Noblet, B. Busson, and C. Humbert, "Diagrammatic theory of linear and nonlinear optics for composite systems," Physical Review A, vol. 104, no. 6, p. 063504, Dec. 2021, doi: 10.1103/PhysRevA.104.063504.

[3] N. Daryakar and C. David, "Thin films of nonlinear metallic amorphous composites," Nanomaterials, vol. 12, no. 19, p. 3359, 2022, doi: 10.3390/nano12193359.

[4] M. Kauranen and A. V. Zayats, "Nonlinear plasmonics," *Nature Photonics*, vol. 6, pp. 737–748, 2012, doi: 10.1038/nphoton.2012.244.

[5] J. Butet, P.-F. Brevet, and O. J. F. Martin, "Optical second harmonic generation in plasmonic nanostructures: from fundamental principles to advanced applications," *ACS Nano*, vol. 9, no. 11, pp. 10545–10562, 2015, doi: 10.1021/acsnano.5b04373.

[6] M. I. Stockman, "Nanoplasmonics: past, present, and glimpse into future," *Optics Express*, vol. 19, no. 22, pp. 22029–22106, 2011, doi: 10.1364/OE.19.022029.

[7] A. Taflove and S. Hagness, *Computational Electrodynamics: The Finite-Difference Time-Domain Method*, 3rd ed. Norwood, MA, USA: Artech House, 2005, pp. 273-329.

[8] H. Wei, J. Feng, L. Ma, and Q. Wang, "Enhanced third-harmonic generation via gold nanospheres localized surface plasmonic resonance," *Journal of Physics D: Applied Physics*, vol. 55, no. 30, p. 305103, 2022, doi: 10.1088/1361-6463/ac654a.

[9] J. E. Sipe and R. W. Boyd, "Nonlinear susceptibility of composite optical materials in the Maxwell–Garnett model," *Physical Review A*, vol. 46, no. 3, pp. 1614–1629, 1992, doi: 10.1103/PhysRevA.46.1614.

[10] R. W. Boyd and J. E. Sipe, "Nonlinear optical susceptibilities of layered composite materials," *Journal of the Optical Society of America B*, vol. 11, no. 2, pp. 297–303, 1994, doi: 10.1364/JOSAB.11.000297.

[11] C. Zhang, J. Zhang, J. Feng, S. Liu, S. Ding, L. Ma, and Q. Wang, "Plasmon-enhanced second harmonic generation of metal nanostructures," *Nanoscale*, vol. 16, pp. 5960–5975, 2024, doi: 10.1039/D3NR06675D.

[12] A. K. Sarychev and V. M. Shalaev, "Electromagnetic field fluctuations and optical nonlinearities in metal–dielectric composites," *Physics Reports*, vol. 335, no. 6, pp. 275–371, 2000, doi: 10.1016/S0370-

[13] N. Kinsey, C. DeVault, A. Boltasseva, and V. M. Shalaev, "Near-zero-index materials for photonics," *Nature Reviews Materials*, vol. 4, pp. 742–760, 2019, doi: 10.1038/s41578-019-0133-0.

[14] O. Reshef, I. De Leon, M. Z. Alam, and R. W. Boyd, "Nonlinear optical effects in epsilon-near-zero media," *Nature Reviews Materials*, vol. 4, pp. 535-551, 2019, https://doi.org/10.1038/s41578-019-0120-5

[15] B.A. Belyaev and V.V. Tyurnev, “Resonances of electromagnetic oscillations in a spherical metal nanoparticle,” *Microwave and Optical Technology Letters*, vol. 58, no. 8, pp. 1883–1886, 2016, doi: 10.1002/mop.29930.

[16] Ö. Aşırım, "Far-IR to deep-UV adaptive supercontinuum generation using semiconductor nano-antennas via carrier injection rate modulation," *Appl. Nanosci.*, vol. 12, no. 1, pp. 1-16, 2021, doi: 10.1007/s13204-020-01648-0.

[17] Y. Yang et al., "A general theoretical and experimental framework for nanoscale electromagnetism," *Nature*, vol. 576, no. 7786, pp. 248-252, 2019, doi: 10.1038/s41586-019-1803-1.

[18] Y. Zhang and Y. Wang, "Nonlinear optical properties of metal nanoparticles: a review," *RSC Adv.*, vol. 7, no. 71, pp. 45129-45144, 2017, doi: 10.1039/c7ra07551k.

[19] X. Liu et al., "Laser heating of metallic nanoparticles for photothermal ablation applications," *AIP Adv.*, vol. 7, no. 2, p. 025308, 2017, doi: 10.1063/1.4977554.

[20] T. Shaaran et al., "High-order-harmonic generation by enhanced plasmonic near-fields in metal nanoparticles," *Phys. Rev. A*, vol. 87, no. 4, Art. no. 041402, 2013, doi: 10.1103/PhysRevA.87.041402.

[21] O. E. Aşırım and M. Kuzuoğlu, "Plasmonic tuning of nano-antennas for super-gain light amplification," J. Phys. Photonics, vol. 6, no. 2, p. 025011, Apr. 2024, doi: 10.1088/2515-7647/ad3d1c

[22] R. Czaplicki, H. Husu, R. Siikanen, J. Mäkitalo, M. Kauranen, J. Laukkanen, J. Lehtolahti, and M. Kuittinen, "Enhancement of second harmonic generation from metal nanoparticles by passive elements," *Phys. Rev. Lett.*, vol. 110, no. 9, pp. 093902, 2013, doi: 10.1103/PhysRevLett.110.093902.

[23] S. Kim, I. Park, S. Kim, and J. Choi, "High harmonic generation in plasmonic nanostructures," in Imaging and Applied Optics Congress, OSA Technical Digest (CD), Optica Publishing Group, 2010, paper MMA2.

[24] S. Wunderlich and U. Peschel, "Plasmonic enhancement of second harmonic generation on metal coated nanoparticles," Opt. Express, vol. 21, no. 16, pp. 18611–18623, Aug. 2013, doi: 10.1364/OE.21.018611

[25] A. Husakou, S.-J. Im, and J. Herrmann, "Theory of plasmon-enhanced high-order harmonic generation in the vicinity of metal nanostructures in noble gases," *Phys. Rev. A*, vol. 83, no. 4, pp. 043839, 2011, doi: 10.1103/PhysRevA.83.043839.

[26] O. E. Aşırım and M. Kuzuoğlu, "Temporal grating of semiconductor nanoantennas for high-density solar energy harvesting," Phys. Scr., vol. 100, no. 6, p. 065537, May 2025, doi: 10.1088/1402-4896/add4b0

[27] X.-Y. Wu, H. Liang, X.-S. Kong, Q. Gong, and L.-Y. Peng, "Enhancement of high-order harmonic generation in two-dimensional materials by plasmonic fields," Phys. Rev. A, vol. 103, no. 4, p. 043117, Apr. 2021, doi: 10.1103/PhysRevA.103.043117.

[28] J. Boroviks, A. D. Gunn, M. R. Freeman, and M. R. Singh, “Demonstration of a plasmonic nonlinear pseudodiode,” *Nano Letters*, vol. 23, no. 8, pp. 3362–3368, Apr. 2023, doi: 10.1021/acs.nanolett.3c00367.

[29] Y. Zhang, C. Wei, F. Gao, D. Lei, and F. Yang, "Revisiting the linear and nonlinear optical properties of nanoparticle-on-mirror–type plasmonic metasurfaces with transformation optics," Phys. Rev. B, vol. 108, no. 20, p. 205408, Nov. 2023, doi: 10.1103/PhysRevB.108.205408

[30] Y. Yan, N. J. Spear, Q. Meng, M. R. Singh, J. E. Macdonald, and R. F. Haglund, "Harmonic generation up to fifth order from Al/Au/CuS nanoparticle films," Nano Lett., vol. 24, no. 16, pp. 5085–5092, Apr. 15, 2024, doi: 10.1021/acs.nanolett.4c00776.

[31] R. A. Ganeev and A. Atvars, “High-order harmonics generation using spherical and non-spherical nanoparticles,” *Nanomaterials*, vol. 14, no. 12, p. 1010, Jun. 2024, doi: 10.3390/nano14121010.

[32] J. Riporto, A. Demierre, V. Kilin, T. Balciunas, C. Schmidt, G. Campargue, M. Urbain, A. Baltuska, R. Le Dantec, J.-P. Wolf, Y. Mugnier, and L. Bonacina, "Bismuth ferrite dielectric nanoparticles excited at telecom wavelengths as multicolor sources by second, third, and fourth harmonic generation," Nanoscale, vol. 10, no. 17, pp. 8146–8152, 2018, doi: 10.1039/C7NR08102B

[33] D. J. Bergman, “Effective medium approximation for nonlinear conductivity of a composite medium,” in Composite Media and Homogenization Theory, G. Dal Maso and G. F. Dell’Antonio, Eds., vol. 5, Progress in Nonlinear Differential Equations and Their Applications. Boston, MA, USA: Birkhäuser, 1991, pp. 67–79, doi: 10.1007/978-1-4684-6787-1_5.

[34] Z. Li et al., "Direct visualization of phase-matched efficient second harmonic and broadband sum frequency generation in hybrid plasmonic nanostructures," Light: Science & Applications, vol. 9, p. 180, 2020, doi: 10.1038/s41377-020-00414-4.

[35] Ö. E. Aşırım and M. Kuzuoglu, "Nanoscale active tuning of the second harmonic generation efficiency in semiconductors from super-low to gigantic values," New J. Phys., vol. 24, p. 083046, 2022, doi: 10.1088/1367-2630/ac8b25.

[36] A. Kumari, M. Aghdaee, M. Van de Voorde, and O. S. Ojambati, "Few photons probe third-order nonlinear properties of nanomaterials in a plasmonic nanocavity," Adv. Opt. Mater., vol. 13, p. 2403484, 2025, doi: 10.1002/adom.202403484

[37] B. E. A. Saleh and M. C. Teich, “Metal and Metamaterial Optics,” in Fundamentals of Photonics, 3rd ed. Hoboken, NJ, USA: Wiley, 2019, ch. 8, pp. 303–352.

[38] R. W. Boyd, “Wave-Equation Description of Nonlinear Optical Interactions,” in Nonlinear Optics, 2nd ed. San Diego, CA, USA: Academic Press, 2003, ch. 2, pp. 69–133.

[39] E. Kim et al., "Nonlinear optical spectroscopy of photonic metamaterials," *Phys. Rev. B*, vol. 78, no. 11, p. 113102, 2008, doi: 10.1103/PhysRevB.78.113102.

[40] A. Rossetti, H. Hu, T. Venanzi, et al., "Control and enhancement of optical nonlinearities in plasmonic semiconductor nanostructures," Light: Science & Applications, vol. 14, p. 192, 2025. [Online]. Available: https://doi.org/10.1038/s41377-025-01783-4

[41] Ma H, Xu J, Shalaev VM, Cai X. Third-order nonlinear properties of Au clusters containing dielectric thin films. In: Shalaev VM, editor. *Optical Properties of Nanostructured Random Media*. Berlin: Springer; 1998. p. 41–56.

[42] Gao L, Li Z-Y. Third-order nonlinear optical response of metal dielectric composites. J Appl Phys. 2000;87(4):1620–1625. doi:10.1063/1.372069.

[43] Lepeshkin NN, Kim W, Safonov VP, Zhu JG, Armstrong RL, White CW, et al. Optical nonlinearities of metal-dielectric composites. J Nonlinear Opt Phys Mater. 1999;08(02):191–210. doi:10.1142/s021886359900014x.

[44] D. Ricard, P. Roussignol, and C. Flytzanis, “Surface-mediated enhancement of optical phase conjugation in metal colloids,” Opt. Lett., vol. 10, no. 10, pp. 511–513, 1985, doi: 10.1364/OL.10.000511.

[45] F. Hache, D. Ricard, C. Flytzanis, and U. Kreibig, “The optical Kerr effect in small metal particles and metal colloids: The case of gold,” Appl. Phys. A, vol. 47, no. 4, pp. 347–357, 1988, doi: 10.1007/BF00615498.

[46] V. M. Shalaev, E. Y. Poliakov, and V. A. Markel, “Small-particle composites. II. Nonlinear optical properties,” Phys. Rev. B, vol. 53, no. 5, pp. 2437–2449, 1996, doi: 10.1103/PhysRevB.53.2437.

[47] R. del Coso, J. Requejo-Isidro, J. Solis, J. Gonzalo, and C. N. Afonso, “Third-order nonlinear optical susceptibility of Cu:Al2O3 nanocomposites: From spherical nanoparticles to the percolation threshold,” J. Appl. Phys., vol. 95, no. 5, pp. 2755–2762, 2004, doi: 10.1063/1.1643779.

[48] A. Lukichev, “Physical meaning of the stretched exponential Kohlrausch function,” *Phys. Lett. A*, vol. 383, no. 24, pp. 2983–2987, 2019, doi: 10.1016/j.physleta.2019.06.029.